Spatial pattern formation and instabilities in resonators with nonlinear dispersive media

L. A. Lugiato
Dipartimento di Fisica, Università degli Studi di Milano, via Celoria 16, 20133 Milano, Italy

Wang Kaige* and N. B. Abraham
Department of Physics, Bryn Mawr College, Bryn Mawr, Pennsylvania 19010-2899
(Received 28 September 1993)

We discuss instabilities of the fundamental single-transverse-mode solution and the formation of new transverse spatial patterns in optical systems, containing nonlinearly absorbing two-level media using two transverse cavity geometries (rectangular and cylindrical). Under the appropriate approximations, these two models can be described by the same set of dynamical equations. Though the equations for the two models differ in their coefficients, their dynamical solutions are comparable. We find hysteresis phenomena associated with transitions in the transverse structure of the intensity which are completely different from the steady-state bistability and hysteresis found in theories of single-mode operation.

PACS number(s): 42.65.Pc, 42.50.−p, 05.70.Ln

I. INTRODUCTION

There has been remarkable development in both theoretical and experimental studies of optical instabilities during the past two decades [1–9]. Most studies have examined the temporal behavior—pulsations or oscillations of the output can appear spontaneously in many optical systems with constant control parameters. More recently, attention has turned to the spontaneous formation of spatial patterns in both absorbing (bistability) and amplifying (laser) nonlinear optical systems [10–35]. Consideration of changing transverse patterns is an unavoidable consequence of studying optical instabilities because the optical field naturally has a transverse variation in any physical system. However, the introduction of transverse spatial coordinates causes mathematical difficulties that, until recently, discouraged extensive work in this area.

Analytical results have been reported for models of cavities with rectangular boundary conditions for both passive optical systems and laser [12,14]. It has been proved, in the study of these models, the new stationary spatial patterns arise by what is called a soft-mode instability, characterized by the vanishing of a real eigenvalue on the instability boundary. For example, studies of a bistable ring resonator (with a nonlinear two-level absorber) have found that complicated two-dimensional, transverse spatiotemporal patterns may be formed with an input pump beam of either a plane wave or a Gaussian transverse spatial profile [16,24]. Laser systems with cylindrical geometry have also been analyzed theoretically and studied experimentally [17(b),20,23,25,34,35].

These systems undergo not only changes in stationary patterns but also transitions to time-dependent solutions. In bifurcation theory, oscillatory instabilities are sometimes termed hard-mode instabilities (Hopf bifurcations) and are characterized by the vanishing on the instability boundary of the real part of a pair of complex-conjugate eigenvalues of the linear stability analysis.

Although soft-mode instabilities and dissipative structures have been extensively investigated in chemical systems, these features have some unique properties when they appear in optical systems. First, one of the primary factors in the formation of spatial patterns in optical systems is diffraction of the electromagnetic field, instead of diffusion as in the chemical systems. In the simplest mathematical models for nonlinear optical systems, a purely imaginary coefficient multiplies the "diffusion term" (transverse Laplacian). Second, optical systems generally include a cavity which provides boundary conditions for the electromagnetic field. Often the field can be written in terms of a specific set of discrete modes. From this point of view, the formation of the spatial patterns is a result of mode-mode interaction and competition. Furthermore, each electromagnetic field mode has a specific operating frequency, and the different transverse modes generally have different frequencies. However, when several transverse patterns are coupled or coexist in a nonlinear dynamical system, they can cooperatively choose a common operating frequency. In autonomous laser systems this phenomenon has been called "cooperative frequency locking." For systems with an externally applied field this is known as "injection locking," while in optical bistability it is more easily understood that the excited transverse modal patterns operate at the frequency of the input field since the media are absorbing and do not autonomously generate fields except when driven into highly nonlinear regimes (see, however, Sec. VI).

There are also two types of bifurcation behavior: supercritical and subcritical. For soft-mode instabilities, it is easier to distinguish these two types of bifurcations by the geometrical structure of the plots of the modal ampli-

*On leave of absence from the Physics Department, Beijing Normal University, Beijing 100875, People's Republic of China.

tudes of the stable stationary solutions versus the bifurcation parameter. For supercritical bifurcations the curves are continuous but their slopes change abruptly (the slope for each amplitude is discontinuous at the bifurcation point). For subcritical bifurcations the plots are discontinuous and hysteresis occurs. Both supercritical and subcritical bifurcations involving soft-mode instabilities have been observed in nonlinear optical systems, and they also appear in our present work.

In addition, a pseudobifurcation, which we term a "soft bifurcation," may also occur. In this case, the plots of the amplitudes of the stationary solutions and their slopes are both continuous but there is a rapid change of slope over a small range of the bifurcation parameter. Then the plot of the results looks like those from a supercritical bifurcation, but on close inspection we can see that these are not from a true bifurcation, because the slope of the curve is still continuous.

In this work we concentrate on passive optical systems with resonators containing nonlinear dispersive media, such as may be used for studies of optical bistability. We model two types of cavity configurations and place the models in a comparable analytic form. Under the appropriate approximations these two models can be described by the same set of dynamical equations, though with different coefficients. This is because the same physical processes govern their behavior. Our numerical results indicate that, when diffraction of the optical field is included, the single-transverse-mode solution that matches the input field profile can be unstable, and inhomogeneous spatial patterns are formed spontaneously at the appropriate level of input intensity. The high transmission branch of the bistable steady-state curve predicted by the single-transverse-mode theory remains stable only in very special situations.

In Sec. II we describe the models. The derivation of the equations for the modal amplitudes is given in Sec. III. In Sec. IV we briefly review the single-transverse-mode steady-state solutions and their linear stability analysis. Numerical results are presented in Sec. V.

II. DESCRIPTION OF THE MODELS

We consider two different transverse geometries for ring cavities, rectangular (or Cartesian) [model 1] and cylindrical [model 2]. Model 1 is, in general, designed for the convenience of theoretical investigations, whereas model 2 is closer to most experimental configurations. The cavity configurations of the two models are shown in Fig. 1.

A. Cavity configurations

Model 1 consists of a ring cavity of length $\mathcal{L}$ with plane mirrors [see Fig. 1(a)]. We assume that the intensity transmission coefficient T of mirrors 1 and 4 is much less than unity, and that mirrors 2 and 3 have 100% reflectivity. The longitudinal coordinate z is measured along the ring; the position of mirror 1 is given by the coordinate $z=0$ at the beginning of the ring and $z=\mathcal{L}$ at the end. The lateral mirrors lie in planes normal to the x axis with a separation distance b and a reflectivity close

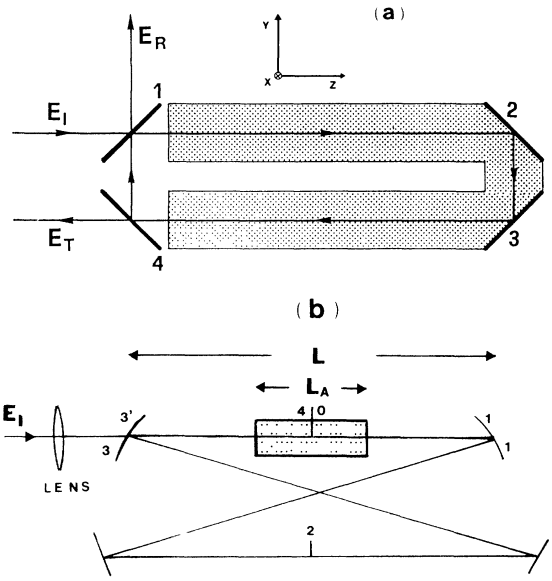

FIG. 1. Schematic representations of the ring cavities. (a) Model 1: Cartesian geometry; (b) model 2: cylindrical geometry, where 1' and 3' indicate the positions after reflection from the mirrors.

to unity. For simplicity, we assume that the y direction is open, and that for TE polarization the transverse field is independent of the y coordinate [12,22(a)]. The extent of the wave in the y direction is not infinite but it is much larger than b.

Model 2 consists of a ring cavity of length $\mathcal{L}$ with two plane mirrors and two spherical mirrors, both with radius of curvature R_0, separated by a distance L. We assume that the transmission coefficient T of the two spherical mirrors is much less than unity and that the two plane mirrors have 100% reflectivity. Position 0 in Fig. 1(b) is the origin of the longitudinal coordinate z and position 2 is the center of symmetry along the longitudinal direction. We assume that the beam is nearly normally incident on the mirrors [the acute angles in Fig. 1(b) are assumed to be very small] and introduce the paraxial approximation [36].

B. Medium

For both models the nonlinear medium (one which is linearly absorbing for weak fields) has a length L_A and volume V. We assume it is a collection of homogeneously broadened two-level atoms with a transition frequency ω_a. The atomic polarization and population relaxation rates are denoted by $\gamma_\perp$ and $\gamma_\parallel$, respectively. For model 1, we assume the medium fills the whole cavity (i.e., $L_A=\mathcal{L}$), but for model 2 we use the thin medium approximation for convenience.

C. Expansion in transverse modes

For model 1, if we assume nearly perfectly reflecting boundary conditions at the side mirrors, the transverse distribution of the optical field can be expanded in terms

of the mode functions

$$g_0(x)=1\ ,$$
$$g_n(x)=2^{1/2}\cos(n\pi x),\quad n=1,2,\ldots, \tag{1}$$

where x has been normalized to the distance b, so that $0\le x\le 1$.

For simplicity we assume cylindrical symmetry for solutions to model 2, and the resulting cavity modes are the Gauss-Laguerre functions [36,37,30]

$$A_n(\rho,\eta)=\frac{2}{v(\eta)}L_n\left[\frac{2\rho^2}{v^2(\eta)}\right]\exp\left\{-\frac{\rho^2}{v^2(\eta)}+i\left[\frac{\rho^2}{u(\eta)}-(2n+1)\tan^{-1}\left[\frac{\eta}{\eta_0}\right]\right]\right\}, \tag{2a}$$

where

$$v(\eta)=\left\{\eta_0\left[1+\left[\frac{\eta}{\eta_0}\right]^2\right]\right\}^{1/2} \tag{2b}$$

and

$$u(\eta)=\frac{1}{\eta}(\eta^2+\eta_0^2)\ . \tag{2c}$$

$L_n(x)$ is the Laguerre polynominal of order n and η_0 is the Fresnel number $(\pi w_0^2/\lambda L)$, where w_0 is the beam waist. Hence the Rayleigh range corresponds to $\eta_0 L$. The normalized cylindrical coordinates are

$$\eta\equiv z/L \tag{3a}$$

and

$$\rho\equiv(k_0/2L)^{1/2}r\ , \tag{3b}$$

with

$$k_0\equiv\omega_0/c\ , \tag{4}$$

where r is the radial coordinate, ω_0 is the frequency of the input field, and c is the speed of light.

D. Input field

For model 1 we take the input to be a homogeneous plane wave of frequency ω_0, matched to the fundamental mode $n=0$. For model 2 the input field is taken to have a Gaussian transverse profile and frequency ω_0. The lens of Fig. 1(b) assures that the Gaussian input beam is matched to the fundamental mode inside the cavity

$$E_{\rm in}(\rho,\eta)\sim A_0(\rho,\eta)\ . \tag{5}$$

III. DERIVATION OF THE FIELD EQUATIONS

The reader who is not interested in the details of the derivation can skip this section and go directly to the beginning of Sec. IV, where a summary of the main steps is provided.

For an atomic system of homogeneously broadened two-level atoms, under the assumptions of a slowly varying envelope, and with the dipole and rotating-wave approximations, the Maxwell-Block equations describing the dynamics of the system are [22(a)]

$$\frac{1}{2ik_0}\nabla_t^2F+\frac{\partial F}{\partial z}+\frac{1}{c}\frac{\partial F}{\partial t}=-\alpha P\ , \tag{6a}$$

$$\frac{\partial P}{\partial t}=\gamma_\perp[DF-P(1+i\Delta)]\ , \tag{6b}$$

and

$$\frac{\partial D}{\partial t}=-\gamma_\parallel[\tfrac{1}{2}(PF^*+FP^*)+D-1]\ , \tag{6c}$$

where $F(x,y,z,t)$ and $P(x,y,z,t)$ are the envelopes of the field and the atomic polarization, respectively, within the rotating frame of the input field. $D(x,y,z,t)$ is the difference between the population of the lower level and the population of the upper level per atom. These functions vary slowly with respect to z and t on the scale of a wavelength or an optical period, respectively. ∇_t^2 is the transverse Laplacian and α is the unsaturated absorption coefficient of the field on resonance,

$$\alpha=\frac{2\pi\mu^2k_0N}{\hbar\gamma_\perp V}\ , \tag{7}$$

where μ is the dipole moment of the atomic transition, N is the total number of atoms, and V is the volume of the medium. The atomic detuning parameter Δ is defined as

$$\Delta\equiv\frac{\omega_a-\omega_0}{\gamma_\perp}\ . \tag{8}$$

The Maxwell-Bloch equations are independent of the cavity configuration. When we select the particular cavity configuration, with its boundary and modal expansion, the corresponding equations for the modal amplitudes are obtained. In order to compare the two models, we use the same symbols for corresponding parameters and variables of both models.

A. Field equations for model 1

1. *Modal equation for the longitudinal mode $m=0$ [22(a)]*

We define the normalized plane-wave input-field amplitude Y by

$$\frac{\boldsymbol{\mu}\cdot\mathbf{E}_{\rm in}}{\hbar}=(\gamma_\perp\gamma_\parallel T)^{1/2}\tfrac{1}{2}\{Y\exp(-i\omega_0 t)+\text{c.c.}\}\ , \tag{9}$$

where $\mathbf{E}_{\rm in}$ is the amplitude of the input field. The boundary condition of the ring cavity of model 1 is

$$F(x,y,0,t)=TY+R\exp(-i\delta_0)F(x,y,\mathcal{L},t)\ , \tag{10}$$

where the reflectivity coefficient is given by

$$R=1-T \ . \tag{11}$$

The cavity detuning parameter δ_0 is given by

$$\delta_0 \equiv \frac{(\omega_c-\omega_0)T}{\kappa} \ , \tag{12}$$

where ω_c is the frequency of the longitudinal cavity mode nearest to ω_0 and κ is the cavity linewidth defined as

$$\kappa=\frac{cT}{\mathcal{L}} \ . \tag{13}$$

As described in Ref. [22(a)], we introduce the uniform field limit (in the longitudinal direction) and the single-longitudinal-mode approximation. The uniform field limit is defined by

$$\alpha L_A \ll 1, \quad T \ll 1, \quad \text{and} \quad |\delta_0| \ll 1 \ , \tag{14}$$

with

$$C \equiv \frac{\alpha L_A}{2T} \quad \text{and} \quad \theta \equiv \frac{\delta_0}{T} \quad \text{arbitrary} \ .$$

If ω_c is also the resonant frequency of the longitudinal mode closest to ω_a and the longitudinal mode spacing $2\pi c/\mathcal{L}$ is much larger than the atomic linewidth $\gamma_\perp$, only the resonant longitudinal mode $m=0$ (in the frame of the input field) can be excited.

The modal amplitude equations for the longitudinal mode $m=0$ is [22(a)]

$$\frac{\partial f^{(0)}}{\partial t}=\kappa[-i\theta f^{(0)}-(f^{(0)}-Y)-2Cp^{(0)}] + i\frac{c}{2k_0 b^2}\frac{d^2 f^{(0)}}{dx^2} \ , \tag{15a}$$

$$\frac{\partial p^{(0)}}{\partial t}=\gamma_\perp[f^{(0)}d^{(0)}-(1+i\Delta)p^{(0)}] \ , \tag{15b}$$

and

$$\frac{\partial d^{(0)}}{\partial t}=-\gamma_\perp[\tfrac{1}{2}(f^{(0)}p^{(0)*}+f^{(0)*}p^{(0)})+d^{(0)}-1] \ , \tag{15c}$$

where $f^{(0)}(x,t)$, $p^{(0)}(x,t)$, and $d^{(0)}(x,t)$ are the field amplitude, the atomic polarization, and the population difference of the longitudinal mode $m=0$, respectively.

2. *Adiabatic elimination of the atomic variables*

On the assumption that

$$\gamma_\perp, \gamma_\parallel \gg \kappa \ , \tag{16}$$

we can adiabatically eliminate the atomic variables $p^{(0)}$ and $d^{(0)}$ from Eq. (15) and obtain the field equation

$$\frac{\partial f^{(0)}}{\partial t'}=Y-f^{(0)}\left[\left[1+\frac{2C}{1+\Delta^2+|f^{(0)}|^2}\right]+i\left[\theta-\frac{2C\Delta}{1+\Delta^2+f^{(0)2}}\right]\right] + ia\frac{d^2 f^{(0)}}{dx^2} \ , \tag{17a}$$

where

$$t' \equiv \kappa t \tag{17b}$$

and

$$a \equiv \frac{1}{4\pi T\mathcal{F}} \ , \tag{17c}$$

with $\mathcal{F}$ being the Fresnel number, $\mathcal{F}=b^2/\lambda\mathcal{L}$. We assume that $\mathcal{F}$ is large so that the parameter a is of order unity. The parameter a characterizes the frequency spacing between the first transverse mode and the fundamental longitudinal cavity mode by [22(a)]

$$a=\frac{\omega_{n=1}-\omega_c}{\pi^2\kappa} \ . \tag{17d}$$

3. *Partial differential equation of motion for model 1*

The cubic approximation for the nonlinearity in Eq. (17a) holds under the condition $1+\Delta \gg |f^{(0)}|^2$. We consider a more restrictive condition which gives greater range for the intensity [38]:

$$|\Delta| \gg 1, \quad 2C/|\Delta| \gg 1, \quad 2C/\Delta^2 \ll 1, \quad \theta-(2C/\Delta) \sim 1 \ . \tag{17e}$$

The cubic approximation consists of retaining only the first two terms of the binomial expansion of the denominator in Eq. (17a), and in neglecting 1 with respect to $i\Delta$ and Δ^2. One then obtains the equation [12]

$$\frac{\partial E}{\partial t'}=E_I-(1+i\bar{\eta}\Theta)E+i\bar{\eta}E|E|^2+ia\frac{d^2E}{dx^2} \ , \tag{18a}$$

where

$$E(x,t')=\left[\frac{2C}{|\Delta|^3}\right]^{1/2} f^{(0)}(x,t') \ , \tag{18b}$$

$$E_I=\left[\frac{2C}{|\Delta|^3}\right]^{1/2} Y \ , \tag{18c}$$

$$\bar{\eta}\Theta=\theta-\frac{2C}{\Delta} \ , \tag{18d}$$

and

$$\Delta=-\bar{\eta}|\Delta| \quad (\bar{\eta}=\pm 1) \ . \tag{18e}$$

The parameter $\bar{\eta}$ carries the sign of the detuning Δ. For $\bar{\eta}=1$ the medium is self-focusing, and for $\bar{\eta}=-1$ it is self-defocusing.

4. *Modal equations for model 1*

For the cavity configuration of model 1, the field amplitude E can be expanded in orthogonal transverse modes,

$$E(x,t')=\sum_{n=0}^{\infty} E_n(t')g_n(x) \ . \tag{19}$$

By substituting Eq. (19) into Eq. (18a), the modal equations are

$$\frac{dE_n}{dt'}=E_I\delta_{n,0}-(1+i\Lambda_n)E_n+i\bar{\eta}\sum_{k,l,m}\Gamma_{nklm}E_kE_lE_m^* , \tag{20}$$

where $\delta_{n,0}$ is the Kronecker delta,

$$\delta_{n,0}=\begin{cases}0, & n\neq 0\\ 1, & n=0\end{cases} , \tag{21a}$$

$$\Lambda_n=\bar{\eta}\Theta+a\pi^2n^2 , \tag{21b}$$

and

$$\Gamma_{nklm}=\int_0^1 g_n(x)g_k(x)g_l(x)g_m(x)dx . \tag{21c}$$

B. Field equations for model 2

Using the normalized variables of Eqs. (3) and $\tau=\gamma_\perp t$, Eqs. (6) become [36]

$$\frac{\partial F}{\partial\eta}+\frac{1}{\nu}\frac{\partial F}{\partial\tau}=\tfrac{1}{4}i\nabla_t^2F-\alpha LP , \tag{22a}$$

$$\frac{\partial P}{\partial\tau}=DF-P(1+i\Delta) , \tag{22b}$$

and

$$\frac{\partial D}{\partial\tau}=-\gamma[\tfrac{1}{2}(PF^*+FP^*)+D-1] , \tag{22c}$$

where

$$\nu=\frac{c}{\gamma_\perp L} , \tag{22d}$$

$$\gamma=\frac{\gamma_\parallel}{\gamma_\perp} , \tag{22e}$$

and

$$\nabla_t^2=\frac{\partial^2}{\partial\rho^2}+\frac{1}{\rho}\frac{\partial}{\partial\rho} . \tag{22f}$$

The slowing varying amplitudes $F(\rho,\eta,\tau)$, $P(\rho,\eta,\tau)$, and $D(\rho,\eta,\tau)$ are independent of the angular coordinate by the assumption that they maintain the cylindrical symmetry of the cavity and input field.

1. Modal expansion

We proceed in a manner different than in our analysis of model 1. First, the field envelope $F(\rho,\eta,\tau)$ is expanded in transverse modes,

$$F(\rho,\eta,\tau)=\sum_n A_n(\rho,\eta)f_n(\eta,\tau) , \tag{23}$$

where the Gauss-Laguerre functions $A_n(\rho,\eta)$ [see Eq. (2)] are the solutions of the differential equation

$$\frac{\partial A_n}{\partial\eta}=\frac{i}{4}\nabla_t^2A_n \tag{24}$$

and obey the orthonormality relation

$$\int_0^\infty d\rho\,\rho A_n^*(\rho,\eta)A_{n'}(\rho,\eta)=\delta_{n,n'} . \tag{25}$$

We substitute Eq. (23) into Eq. (22a) for the field equation and use the atomic equations. The new field equations for the modal amplitudes $f_n(\eta,\tau)$ are

$$\frac{\partial f_n}{\partial\eta}+\frac{1}{\nu}\frac{\partial f_n}{\partial\tau}=-\alpha L\int_0^\infty d\rho\,\rho A_n^*(\rho,\eta)P(\rho,\eta,\tau) . \tag{26}$$

2. Boundary conditions

For the ring cavity of model 2 with an input field, the appropriate boundary conditions for the mode amplitudes $f_n(\eta,\tau)$ are (see Appendix A)

$$f_n\left[-\frac{1}{2},\tau\right]=TY\delta_{n,0}+\exp(-i\delta_n)Rf_n\left[\frac{1}{2},\tau-\gamma_\perp\frac{\mathcal{L}-L}{c}\right] . \tag{27}$$

The normalized input amplitude Y is defined by the input field $\mathbf{E}_{\rm in}(t)$, which is assumed to be matched to the fundamental mode $n=0$,

$$\frac{\boldsymbol{\mu}\cdot\mathbf{E}_{\rm in}(t)}{\hbar}=(\gamma_\perp\gamma_\parallel T)^{1/2}\frac{1}{2}\left[YA_0\left[\rho,-\frac{1}{2}\right]\exp\left\{i\left[k_0\left[-\frac{L}{2}\right]-\omega_0t\right]\right\}+\text{c.c.}\right] , \tag{28}$$

and the parameter δ_n is

$$\delta_n=\frac{(\omega_n-\omega_0)\mathcal{L}}{c} , \tag{29}$$

where ω_n is the frequency of the nth transverse mode,

$$\omega_n=\omega_c+\phi_n\frac{c}{\mathcal{L}} . \tag{30}$$

In Eq. (30), $2\phi_n$ is the phase shift of the nth transverse mode after a round trip,

$$\phi_n=2(2n+1)\left[\tan^{-1}\left[\frac{1}{2v_0^2}\right]+\tan^{-1}\left[\frac{\mathcal{L}^{-1}-1}{2v_2^2}\right]\right] , \tag{31}$$

where $v_0^2=\eta_0$ and v_2^2 are the Rayleigh range (normalized to L) at the positions 0 and 2, respectively [see Fig. 1(b)], and $\mathcal{L}\equiv L/\mathcal{L}$ [30,37].

In order to obtain simple modal equations, we perform the following transformations to arrive at periodic

boundary conditions. First, let

$$\tau' \equiv \tau + \gamma_\perp(\eta+\tfrac{1}{2})\frac{\mathcal{L}-L}{c} , \tag{32a}$$

$$f_n'(\eta,\tau') \equiv f_n(\eta,\tau) , \tag{32b}$$

$$F'(\rho,\eta,\tau') \equiv F(\rho,\eta,\tau) , \tag{32c}$$

$$P'(\rho,\eta,\tau') \equiv P(\rho,\eta,\tau) , \tag{32d}$$

$$D'(\rho,\eta,\tau') \equiv D(\rho,\eta,\tau) . \tag{32e}$$

Then the modal equations become

$$\frac{\partial f_n'}{\partial \eta} + \frac{\gamma_\perp \mathcal{L}}{c}\frac{\partial f'n}{\partial \tau'} = -\alpha L \int_0^\infty d\rho\, \rho\, A_n^*(\rho,\eta) P'(\rho,\eta,\tau') , \tag{33a}$$

$$\frac{\partial P'}{\partial \tau'} = D'F' - P'(1+i\Delta) , \tag{33b}$$

$$\frac{\partial D'}{\partial \tau'} = -\gamma[\tfrac{1}{2}(P'F'^* + F'P'^*) + D' - 1] , \tag{33c}$$

and the boundary conditions Eq. (27) are

$$f_n'(-\tfrac{1}{2},\tau') = TY\delta_{n,0} + \exp(-i\delta_n) R f_n'(\tfrac{1}{2},\tau') . \tag{34}$$

Then, we define the new modal amplitudes $\bar{f}_n(\eta,\tau')$,

$$f_n'(\eta,\tau') \equiv [\bar{f}_n(\eta,\tau') - TY\delta_{n,0}(\eta+\tfrac{1}{2})] \times \exp[-(\ln R - i\delta_n)(\eta+\tfrac{1}{2})] , \tag{35}$$

which obey periodic boundary conditions

$$\bar{f}_n(-\tfrac{1}{2},\tau') = \bar{f}_n(\tfrac{1}{2},\tau') . \tag{36}$$

3. *Longitudinal average of the modal amplitudes*

Using the definitions in Eqs. (35), the field equations become

$$\frac{\partial \bar{f}_n(\eta,\tau')}{\partial \eta} + \frac{\gamma_\perp \mathcal{L}}{c}\frac{\partial \bar{f}_n(\eta,\tau')}{\partial \tau'} = TY\delta_{n,0} - TY\delta_{n,0}(\eta+\tfrac{1}{2})(\ln R - i\delta_n) + (\ln R - i\delta_n)\bar{f}_n(\eta,\tau') - \exp[(\eta+\tfrac{1}{2})(\ln R - i\delta_n)]\alpha L \int_0^\infty d\rho\, \rho\, A_n^*(\rho,\eta) P'(\rho,\eta,\tau') . \tag{37}$$

Defining the longitudinal averages of the field amplitudes of the transverse modes

$$\bar{f}_n(\tau') \equiv \int_{-1/2}^{1/2} d\eta\, \bar{f}_n(\eta,\tau') , \tag{38}$$

and using the periodic boundary conditions of Eqs. (36), we integrate Eqs. (37) with respect to η over the range $(-\frac{1}{2},\frac{1}{2})$ with the results

$$\frac{\gamma_\perp \mathcal{L}}{c}\frac{\partial \bar{f}_n(\tau')}{\partial \tau'} = TY\delta_{n,0} - \tfrac{1}{2}TY\delta_{n,0}(\ln R - i\delta_n) + (\ln R - i\delta_n)\bar{f}_n(\tau') - \alpha L_A I_n(\tau') , \tag{39}$$

where the integrals $I_n(\tau')$ are

$$I_n(\tau') \equiv \frac{L}{L_A}\int_{-1/2}^{1/2} d\eta \exp[(\ln R - i\delta_n)(\eta+\tfrac{1}{2})] \times \int_0^\infty d\rho\, \rho\, A_n^*(\rho,\eta) P'(\rho,\eta,\tau') . \tag{40}$$

4. *Some approximations*

a. Uniform field limit. We use the uniform field limit as described by Eq. (14) and introduce the assumption that the frequency difference between the relevant nonresonant transverse modes and the input frequency ω_0 is much smaller than the free spectral range, precisely [39]

$$\delta_n = \frac{\omega_n - \omega_0}{c/\mathcal{L}} \sim O(T) \ll 1, \quad n \geq 1 . \tag{41}$$

This hypothesis requires that the Fresnel number η_0 is on the order of $(1/T)$. Condition (41) implies that the dynamics of the system is governed by modes with a single value of the longitudinal modal index m (see Sec. III B 4 b below). The field modal amplitude equations (39) become

$$\frac{1}{\kappa'}\frac{\partial \bar{f}_n(\tau')}{\partial \tau'} = Y\delta_{n,0} - \left[1 + i\frac{\delta_n}{T}\right]\bar{f}_n(\tau') - 2CI_n(\tau') , \tag{42a}$$

where

$$\kappa' = \frac{cT}{\gamma_\perp \mathcal{L}} . \tag{42b}$$

b. Single-longitudinal-mode approximation. By the periodic boundary conditions Eqs. (36), $\bar{f}_n(\eta,\tau')$ can be expanded in the form

$$\bar{f}_n(\eta,\tau') = \sum_m f_n^{(m)}(\tau')\exp(i2\pi m\eta) . \tag{43}$$

In the approximation Eq. (41) of a single longitudinal mode, all the modal amplitudes with $m \neq 0$ can be neglected, so that

$$\bar{f}_n(\eta,\tau') = f_n^{(0)}(\tau') = \bar{f}_n(\tau') . \tag{44}$$

c. Adiabatic elimination of the atomic variables, cubic approximation, and thin-medium approximation. Under these approximations the integrals become (see Appendix B)

$$I_n(\tau') \cong -\frac{i}{\Delta} f_n^{(0)}(\tau') + \frac{i}{\eta_0 \Delta^3}\sum_{k,l,m} \Gamma_{nklm} f_k^{(0)}(\tau') f_l^{(0)}(\tau') f_m^{(0)*}(\tau') , \tag{45}$$

where ($\bar{\rho} = \rho/\eta_0^{1/2}$)

$$\Gamma_{nklm}=\int_0^\infty d\bar{\rho}\,\bar{\rho}\,A_n(\bar{\rho})A_k(\bar{\rho})A_l(\bar{\rho})A_m(\bar{\rho}) \tag{46a}$$

and

$$A_n(\bar{\rho})=2L_n(2\bar{\rho}^2)\exp(-\bar{\rho}^2)\ . \tag{46b}$$

5. *Final modal equations*

By Eqs. (29)–(31), the mode detuning parameter becomes

$$\begin{aligned}\frac{\delta_n}{T}&=\frac{(\omega_{n=0}-\omega_0)\mathcal{L}}{cT}+\frac{(\omega_n-\omega_{n=0})\mathcal{L}}{cT}\\&=\frac{\delta_0}{T}+\frac{2n\phi_0}{T}\\&=\theta+an\ ,\end{aligned} \tag{47a}$$

where θ is given by Eq. (14) and

$$a\equiv\frac{2\phi_0}{T}=\frac{(\omega_{n=1}-\omega_{n=0})}{\kappa}\ . \tag{47b}$$

The parameter a characterizes the frequency spacing between the transverse modes.

Now we renormalize the variables using

$$t'=\kappa'\tau'\ , \tag{48a}$$

$$E_n=\left[\frac{2C}{\eta_0|\Delta|^3}\right]^{1/2}f_n^{(0)}\ , \tag{48b}$$

$$E_I=\left[\frac{2C}{|\Delta|^3\eta_0}\right]^{1/2}Y\ , \tag{48c}$$

and define the detuning parameter $\bar{\eta}\Theta$ as in Eq. (18d). Then the final modal equations of the field have the same form as for model 1, i.e., Eq. (20), with the exceptions that the coefficients of the linear term are now

$$\Lambda_n=\bar{\eta}\Theta+an\ , \tag{49}$$

and the coefficients of the cubic terms, Γ_{nklm}, are given by Eqs. (46) instead of Eq. (21c).

6. *Partial differential equation of motion for model 2*

It is possible to construct in an equivalent manner the field equation of motion in the form of a partial differential equation using the modal equations, Eqs. (20), (46), and (49) (see [30])

$$\begin{aligned}\frac{\partial E(\bar{\rho},t')}{\partial t'}&=E_I A_0(\bar{\rho})-(1+i\bar{\eta}\Theta)E(\bar{\rho},t')\\&\quad+i\bar{\eta}E(\bar{\rho},t')|E(\bar{\rho},t')|^2\\&\quad+i\frac{a}{2}(\tfrac{1}{4}\bar{\nabla}_t^2-\bar{\rho}^2+1)E(\bar{\rho},t')\ ,\end{aligned} \tag{50a}$$

where

$$E(\bar{\rho},t')=\sum_n E_n(t')A_n(\bar{\rho}) \tag{50b}$$

and $\bar{\nabla}_t^2$ is defined by Eq. (22f) with ρ replaced by $\bar{\rho}=\rho/\eta_0^{1/2}$. As a matter of fact, if one inserts Eq. (50b) into Eq. (50a) and takes into account the identity

$$(\tfrac{1}{4}\bar{\nabla}_t^2-\bar{\rho}^2+1)A_n(\bar{\rho})=-2nA_n(\bar{\rho})\ , \tag{51a}$$

the orthonormality relation

$$\int_0^\infty d\bar{\rho}\,\bar{\rho}\,A_n(\bar{\rho})A_{n'}(\bar{\rho})=\delta_{n,n'}\ , \tag{51b}$$

and definitions (46a) and (49), one obtains Eqs. (20).

We observe finally that Eqs. (18a), (20), and (50a) can be used to model nonlinear phenomena in a Fabry-Pérot cavity instead of a ring cavity, provided that one introduces the following changes: (a) The parameters κ and C are defined as

$$\kappa\equiv\frac{cT}{2L}\quad\text{and}\quad C\equiv\frac{\alpha L_A}{2T}\ ,$$

where L is the distance between the two spherical mirrors, and the parameter a denotes the frequency spacing between adjacent transverse modes, normalized to $\pi^2\kappa$ in model 1 and to κ in model 2 [see Eq. (17d) and (47b)]; and (b) the right-hand sides of Eqs. (18b), (18c), (48b), and (48c) must be multiplied by $\sqrt{3}$ [see Ref. [22(a)], Sec. IV, and introduce the cubic approximation].

IV. SINGLE-TRANSVERSE MODE STATIONARY SOLUTIONS AND THEIR STABILITIES

Because the derivatives carried out in the previous sections are lengthy and cumbersome, let us now summarize them. We started from the Maxwell-Bloch equations (6) and assumed the limits of small absorption, a high-finesse cavity, and quasiresonance of the input field with one longitudinal mode of the cavity and with its higher-order transverse modes [see Eqs. (14) and (41)]; these conditions allowed us to eliminate the longitudinal variable from the model. We then performed the adiabatic elimination of the atomic variables on the basis of condition (16) and finally, assuming a large atomic detuning [Eqs. (17e)], we performed the cubic approximation. In this way we arrived at a relatively simple partial differential equation for the field envelope [Eq. (18e) for the Cartesian case and Eq. (50a) for the cylindrical case] or, equivalently, to a set of ordinary differential equations for the modal amplitudes [Eq. (20) with Eq. (21b) in the Cartesian case, and with Eq. (49) in the cylindrical case].

When diffraction of the beam is introduced in the models, one of the most important issues is the stability of the fundamental stationary solution which matches the input field. For model 1, analytical results have been presented previously [12,15]. The input field is transversely homogeneous and Eqs. (18) and (20) admit an exactly homogeneous stationary solution, in which $E(x,t')\equiv E_S=E_0$, and all the other amplitudes E_n with $n\neq 0$ vanish. This steady-state equation is [40]

$$|E_I|^2=|E_S|^2[1+(|E_S|^2-\Theta)^2]\ . \tag{52}$$

Note that E_0 corresponds to excitation of only the fundamental mode of the rectangular cavity. The plot of the steady-state solution $|E_S|^2$ vs $|E_I|^2$ has a characteristic S

shape and becomes multivalued when $\Theta^2>3$. The homogeneous solution E_S is unstable with respect to perturbation of the amplitude of the nth mode, provided the following condition is satisfied [12]:

$$|E_S|^2(-)\leq|E_S|^2\leq|E_S|^2(+)\ , \tag{53a}$$

where

$$|E_S|^2(\pm)=\tfrac{2}{3}[\Theta+\bar{\eta}a(n)]\pm\tfrac{1}{3}\sqrt{[\Theta+\bar{\eta}a(n)]^2-3} \tag{53b}$$

and

$$a(n)\equiv a\pi^2n^2\ . \tag{53c}$$

For $n=0$, condition (53a) defines the negatively sloped portion of the steady-state curve Eq. (52), which exists for $\Theta>\sqrt{3}$ [40]. For $n>0$, condition (53a) defines the part of the steady-state curve which is unstable under perturbation with the spatial configuration of mode n. This part exists provided that $\Theta+\bar{\eta}a(n)>\sqrt{3}$. Note from Eq. (53b) that the instability condition for mode n coincides with the condition of negative slope, provided Θ is replaced by $\Theta+\bar{\eta}a(n)$ [see Ref. [22(a)]].

The instability for modal amplitudes with $n>0$ leads usually to the appearance of inhomogeneous stationary solutions, as we will see in the following section. This phenomenon corresponds to the simultaneous breaking of the translational symmetry in space and of the parity symmetry under the transformation $x\rightarrow(1-x)$ (remember that $0\leq x\leq 1$). As a matter of fact, two inhomogeneous stationary solutions appear simultaneously, and one is obtained from the other by the parity transformation [12,22(b)]. Therefore the two solutions have the same modal intensities $|E_n|^2$. When only even modes contribute to the spatial configuration, the two solutions coincide; when odd modes also contribute, the two solutions are different and there is a trivial kind of bistability between them, which may be washed out in the presence of noise [41].

For model 2 there is no homogeneous solution satisfying Eq. (50), since a homogeneous solution cannot match the mirror curvature. However, there is a lowest-order mode and so it makes sense to compare the phenomena for the two models with respect to the amplitude of an input field which is mode matched to the fundamental cavity mode, as assumed in Eq. (50). Although Eqs. (20) for model 2 [i.e., Eqs. (46) and (49)] admit an exact single-mode stationary solution in which all the modal amplitudes E_n with $n\neq 0$ vanish exactly, this solution is unfortunately always unstable since even the slightest nonlinearity distorts the transverse pattern from that of the fundamental mode. This feature arises from the couplings of the mode amplitudes introduced by the coefficients Γ_{nklm} in Eq. (46). However, for small values of the input intensity there is a stable solution which is predominantly the fundamental mode with only small nonzero amplitudes for higher-order modes (Sec. V B). Some characteristics of the stable solution can be observed from the analytic form of the unstable (but approximately similar) fundamental mode solution given by

$$E_I=E_0[1+i\bar{\eta}(\Theta-\Gamma_{0000}|E_0|^2)]\ . \tag{54a}$$

Taking into account that $\Gamma_{0000}=2$ and replacing E_0 by E_S, one has the steady-state equation

$$|E_I|^2=|E_S|^2[1+(2|E_S|^2-\Theta)^2]\ . \tag{54b}$$

The curve of steady-state solutions $|E_S|^2$ vs $|E_I|^2$ is multivalued when $\Theta^2>3$. Note that in terms of the variable $E_S'=\sqrt{2}E_S$, Eq. (54b) becomes identical to Eq. (52).

Linear stability analysis of this solution or of the similar stable solution is hard to complete analytically because of the approximate nature of Eq. (54b), and because of the couplings introduced by the coefficients (46). Instead of the simplicity of the orthogonality relation for Γ_{nklm} in the Cartesian model, we have mode mixing even when Eq. (20) is linearized around Eq. (54a). Hence the linearized equations are not diagonalized.

V. NUMERICAL RESULTS

A. Model 1

We integrate the modal equations, Eqs. (20), until the system reaches a stationary state, and then we adiabatically change the amplitude of the input field. To reduce the integration time necessary to obtain these diagrams, usually we included in our calculations only the first three modes, $n=0,1,2$. As we show in the following by two examples (Figs. 3 and 11), the overall picture as summarized in Sec. VI is not affected by this restriction and, for a certain range of values of the input intensity $|E_I|^2$, even the quantitative description provided by the three-mode model is basically correct.

For model 1, we solve Eqs. (20) together with Eqs. (21b) and (21c). Figure 2 shows the mode intensities $|E_n|^2$ as functions of the homogeneous steady-state intensity $|E_S|^2$, for the parameters $\bar{\eta}=1$, $a\pi^2=1.0$, and $\Theta=1.0$. The infinite set of modal equations is truncated to the first three modes. Because, in this case, the curve of the homogeneous steady-state solutions, $|E_S|^2$ vs $|E_I|^2$, is single valued, we choose $|E_S|^2$ as the abscissa, instead of $|E_I|^2$. Figure 2 indicates that all the bifurcations to nonhomogeneous transverse spatial patterns are supercritical, in accord with the analysis of Ref. [12], which predicts a supercritical bifurcation for $\Theta<\frac{41}{30}\approx 1.4$. In the range $1.0<|E_S|^2<1.67$ the homogeneous solution is unstable with respect to perturbations of the mode $n=1$. A small stable "island," where the homogeneous steady-state solution recovers stability, appears in the range $1.67<|E_S|^2<1.77$, as shown in Fig. 2(b). For $|E_S|^2>1.77$, the homogeneous solution is unstable again, but with respect to perturbations of the mode $n=2$; the second mode grows while the amplitude of the first mode remains zero. The values of the bifurcation points coincide exactly with the predictions of the linear stability analysis. The existence of the stable island is because the instability ranges with respect to perturbations of the modes $n=1$ and $n=2$ [given by Eqs. (53)] do not overlap for the values of the parameters we have selected. At a larger detuning $\Theta=2.0$, the bifurcation behavior is different and more complicated, as shown in Fig. 3. In order to illustrate this explicitly, we also plot the unstable

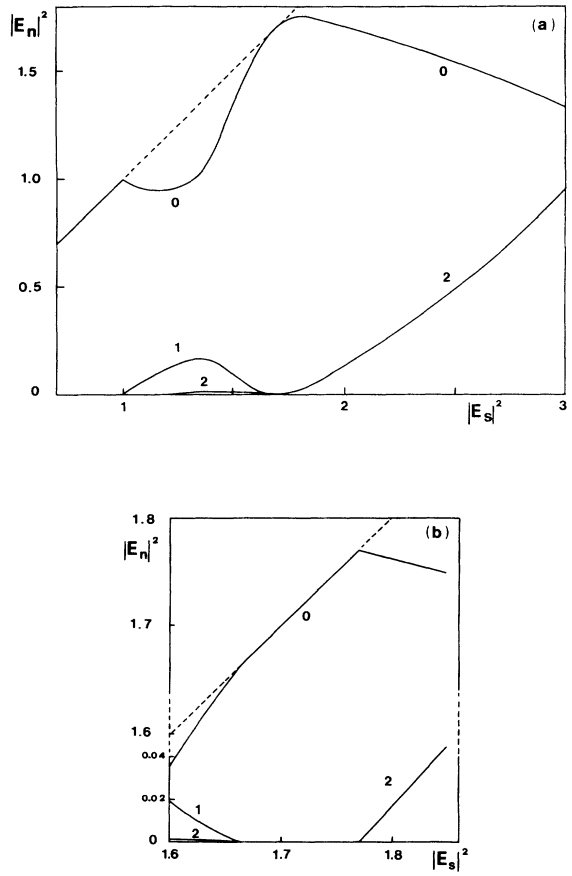

FIG. 2. (a) Stationary-mode intensities as a function of the homogeneous steady-state output intensity of model 1 for $\bar{\eta}=1$, $a\pi^2=1.0$, and $\Theta=1.0$; (b) Magnification of the region around the stable island. In Figs. 2–13 the integer numbers indicate the modal index n.

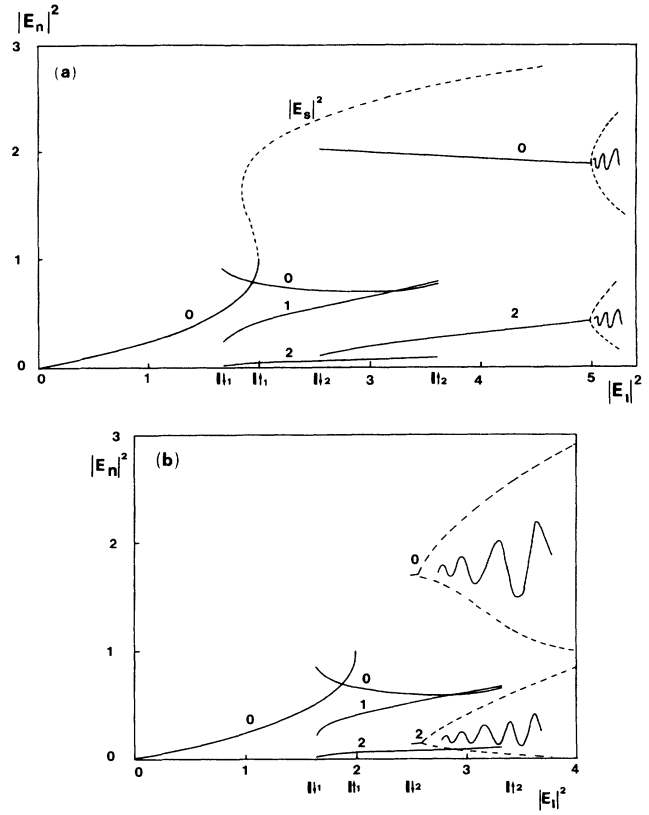

FIG. 3. Mode intensities as a function of the input-field intensity of model 1 for $\bar{\eta}=1$, $a\pi^2=1.0$, and $\Theta=2.0$. The rightmost part of the curves indicates the time-dependent solution. The dashed line indicates the homogeneous stationary solution. (a) Solutions for the model truncated to the first three modes; transition points: $I_{\uparrow 1}=2.01$, $I_{\downarrow 1}=1.67$, $I_{\uparrow 2}=3.63$, $I_{\downarrow 2}=2.54$. (b) Solutions for the model truncated to the first eight modes; transition points: $I_{\uparrow 1}=2.01$, $I_{\downarrow 1}=1.63$, $I_{\uparrow 2}=3.33$, $I_{\downarrow 2}=2.49$.

region according to Eqs. (53) in Fig. 4, in which the shaded part indicates the unstable region corresponding to the negatively sloped of the curve of the steady-state solution of $|E_S|^2$ as a function of $|E_I|^2$ governed by Eq. (52). As we adiabatically increase the input field, the first critical point is $|E_I|^2=2.0$ (i.e., $|E_S|^2=1.0$), which corresponds to the right turning point of the homogeneous steady-state curve. Here the homogeneous steady-state solution of the lower branch becomes unstable with respect to perturbations of the mode $n=0$, and the system would jump to the upper branch of the homogeneous steady-state solutions if there were no perturbations of the inhomogeneous modes. But the homogeneous steady-state solution on the upper branch (which corresponds to the value $|E_S|^2=2.0$) is unstable against perturbations of mode $n=1$, as indicated in Fig. 4; hence the system approaches an inhomogeneous stationary solution.

Figure 3 shows two bistability regions: the first corresponds to a bistability between the lower branch of homogeneous solutions and an inhomogeneous pattern; the second corresponds to bistability between a pattern which is symmetric with respect to the parity transformation $x\rightarrow(1-x)$ and an asymmetric pattern. For large input field intensities $|E_I|^2>5.0$, time-dependent solutions (spatiotemporal structures) occur. Figure 3(b) shows the solution if one includes eight modes in the description. There is no significant difference for the first bistability region, but in the second region the time-dependent solution appears at a much smaller input-field intensity than in Fig. 3(a).

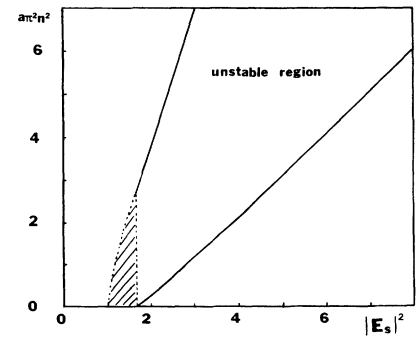

FIG. 4. Unstable domain in the plane of variables $a(n)=a\pi^2n^2$ and $|E_S|^2$ for the same parameters as Fig. 3. The shaded part indicates the unstable region corresponding to the negative slope of the curve $|E_S|^2\sim|E_I|^2$.

B. Model 2

For model 2, when the input field is small enough we find the solution which is approximately the single-fundamental-mode solution (54b). The higher modes are nonzero but negligible. Figure 5 shows the mode intensities as a function of $|E_S|^2$, which is related to the input field by Eq. (54b), from the parameters $\bar{\eta}=1$, $a=1.0$, and $\Theta=1.0$. Although there are points near $|E_S|^2\approx 0.2$ and $|E_S|^2\approx 1.3$ where the curves rapidly change slopes, there are no bifurcations in a rigorous sense, as one sees by checking the value of the determinant of the characteristic matrix of the linear stability analysis at the "bifurcationlike" point. (The determinant appears to have a minimum but does not vanish.) The minimum of the determinant of the characteristic matrix indicates a kind of "soft-bifurcation" behavior. The feature of the first soft bifurcation is that the amplitudes of modes $n>0$ grow noticeably; this feature is comparable to that observed for model 1 (see Fig. 2); the feature of the second soft bifurcation is that the intensity of mode $n=1$ decreases.

As the detuning is increased, the soft-bifurcation feature becomes pronounced until the intensity curves break and become discontinuous; at this point true subcritical bifurcations occur. The first true bifurcation arises for $\Theta=1.5$ and the second for $\Theta=1.6$, as shown in Figs. 6 and 7, respectively. Where the intensity curves become discontinuous, hysteresis appears, as shown in Fig. 6(b), which is a magnification of the region around the first bifurcation of Fig. 6(a). Figure 6(c) shows the magnified region around the second bifurcation, which is still soft but near to becoming a true bifurcation.

As the detuning is increased further, the hysteresis regions are enlarged. Figures 8 and 9 illustrate the steady-state intensities of the modes as functions of the input field $|E_I|^2$ for $\Theta=2.0$ and 4.0, respectively. Figure 10 shows the transverse intensity profiles at the upwards transition points for $\Theta=4.0$, where Fig. 10(a) is for the transition point $I_{\uparrow 1}=4.000\,25$ of the first loop and Fig. 10(b) is for $I_{\uparrow 2}=24.932$ of the second loop. In Fig. 10(a) the narrowing of the region of high intensity indicates the appearance of the Gauss-Laguerre modes different from the fundamental.

With the same parameters as in Fig. 8, we integrate the modal equations of model 2 with six modes and the numerical results are shown in Fig. 11(a). Comparing Figs. 8 and 11(a), there are no major qualitative differences, but the bifurcations occur at smaller values of the input field in Fig. 11(a).

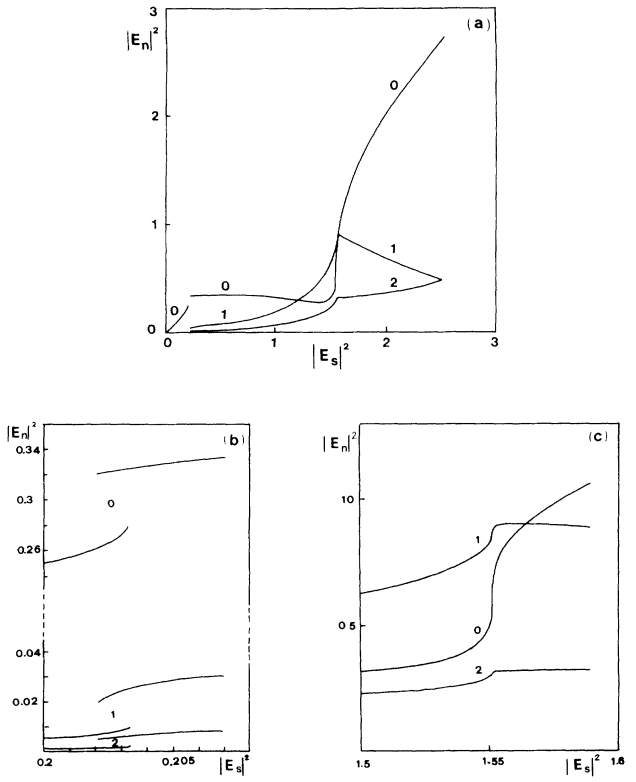

FIG. 6. Mode intensities as a function of $|E_S|^2$ for model 2, truncated to the first three modes. The parameters are $\bar{\eta}=1$, $a=1.0$, and $\Theta=1.5$. (b) and (c) are the magnifications around the transition areas of (a).

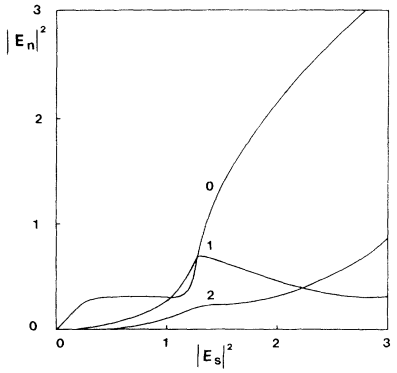

FIG. 5. Mode intensities as a function of $|E_S|^2$ for model 2, truncated to the first three modes. The parameters are $\bar{\eta}=1$, $a=1.0$, and $\Theta=1.0$.

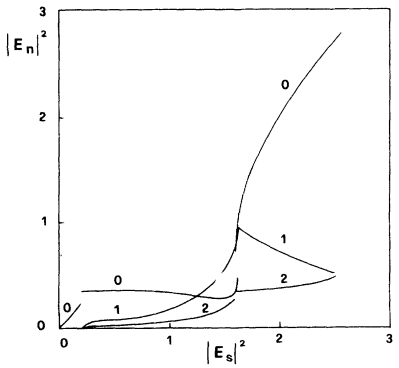

FIG. 7. Mode intensities as a function of $|E_S|^2$ for model 2, truncated to the first three modes. The parameters are $\bar{\eta}=1$, $a=1.0$, and $\Theta=1.6$.

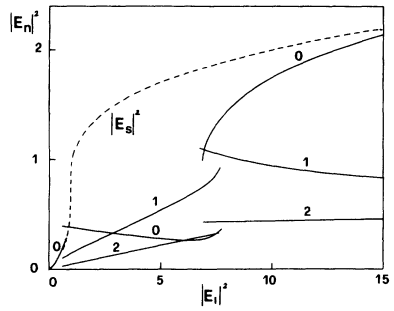

FIG. 8. Mode intensities as a function of input-field intensity for model 2, truncated to the first three modes. The parameters are $\bar{\eta}=1$, $a=1.0$, and $\Theta=2.0$. The dashed line indicates the curve described by Eq. (54b).

Unlike Fig. 3(b) of model 1, where eight operating modes were used, in Fig. 11(a) the amplitudes of the higher-order modes are not negligible. This may create worries about the convergence of the solution when the number of modes is increased. In order to account for the possibility of higher losses for the higher-order modes in the cavity, such as may occur due to the presence of apertures and finite transverse extent of other intracavity elements and of the mirrors themselves, we introduce an additional damping term βn^4 (compare with Ref. [20]) in the modal equations, which take the form

$$\frac{dE_n}{dt'}=E_I\delta_{n,0}-(1+\beta n^4+i\Lambda_n)E_n +i\bar{\eta}\sum_{k,l,m}\Gamma_{nklm}E_kE_lE_m^* , \tag{55}$$

where β is the damping coefficient. These additional losses for the higher-order modes also have the computational advantage of improving the convergence of the modal expansion, justifying the more rapid truncation of the infinite series to a finite number of modal amplitudes.

Figures 11(b) and 11(c) show the results of integrating Eqs. (55) for $\beta=0.005$ and 0.05, respectively. In Fig. 11(c) the intensities of the higher-order modes are obviously diminished. However, the decrease of the amplitudes of the higher-order modes can reduce the width of the bistable regions, and can even eliminate a bifurcation, as shown in Figs. 11(b) and 11(c).

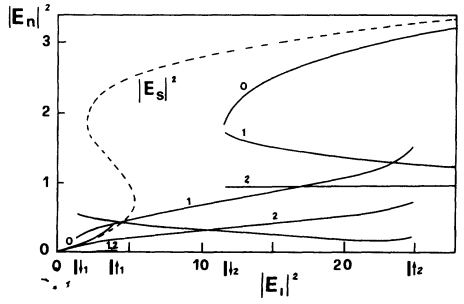

FIG. 9. Mode intensities as a function of input-field intensity for model 2, truncated to the first three modes. The parameters are $\bar{\eta}=1$, $a=1.0$, and $\Theta=4.0$. The transition points are $I_{\uparrow 1}=4.0025$, $I_{\downarrow 1}=1.2506$, $I_{\uparrow 2}=24.932$, $I_{\downarrow 2}=11.625$. The dashed line is the curve of the steady-state solution described by Eq. (54b).

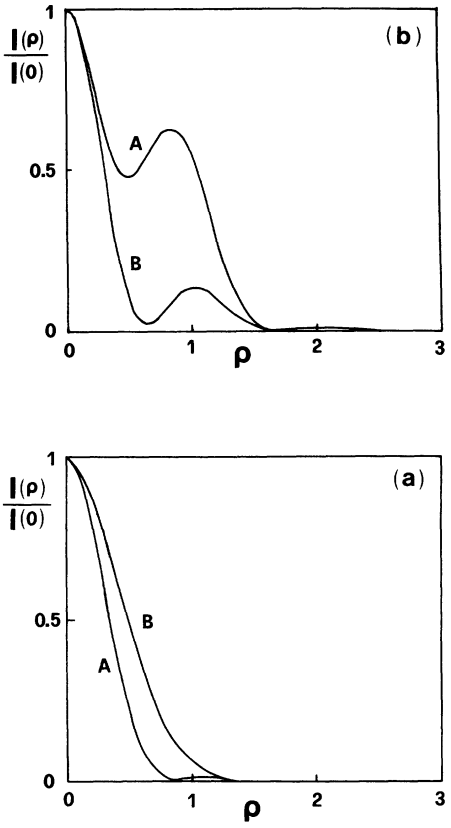

FIG. 10. Transverse intensity profiles at the transition points (a) $I_{\uparrow 1}=4.0025$ and (b) $I_{\uparrow 2}=24.932$ of Fig. 9, where B and A indicate the profiles just before and after the transitions, respectively, when the input intensity is increased.

C. Self-defocusing cases ($\bar{\eta}=-1$)

For the self-defocusing case with model 1, as indicated in Ref. [12], the instability of the transverse homogeneous solution can arise only for $\Theta>2$. With the parameters $\Theta=4.0$, $\bar{\eta}=-1$, and $a\pi^2=1.0$, the numerical results indicate that there are no stable stationary inhomogeneous solutions, as shown in Fig. 12. As a matter of fact, according to Eq. (53), only perturbations of the first transverse mode can provoke the instability of the homogeneous solution. The unstable range, $1.1835<|E_S|^2<2.8165$, is mostly in the region of the negative slope of the steady-state curve, and partly in the lower branch of the homogeneous solution. On the other hand, the upper branch of the homogeneous solution remains stable. Therefore, under perturbations of the first mode, the instability of the lower branch occurs before reaching the turning point, and the system jumps up to the stable upper branch. In other words, the inhomogeneous mode plays the role of a trigger for switching, but there are no stable inhomogeneous patterns which it can create. This effect may go unnoticed in experiments, since patterns during switching transients are rarely studied.

Figure 13 shows the self-defocusing case for model 2 for $\Theta=4.0$, $\bar{\eta}=-1$, and $a=1.0$. The basic bifurcation behavior remains similar to that of the self-focusing case, but the size of the bistable hysteresis regions is greatly decreased with respect to the same case with $\bar{\eta}=1$ (see Fig. 9).

VI. CONCLUDING REMARKS AND DISCUSSION

We have investigated two typical cavity geometries for optical systems containing nonlinearly absorbing two-level media, and we have given a basis for their comparison. We find that, under appropriate approximations, these two models can be described by a set of nonlinear modal equations with different coefficients. Despite rather complicated derivations, from the physical standpoint the structure of the modal equations (20) is simple and understandable. They consist of three parts: the input field, the linear absorptive and dispersive term, and third-order terms representing nonlinear phase shifts. The input part corresponds to the injection of a field matched to the fundamental mode. The coefficient of the first-order term is a complex number: the real part (-1) indicates the cavity damping; and the imaginary part consists of the detuning of the transverse mode's frequency with respect to the input frequency, shifted by the

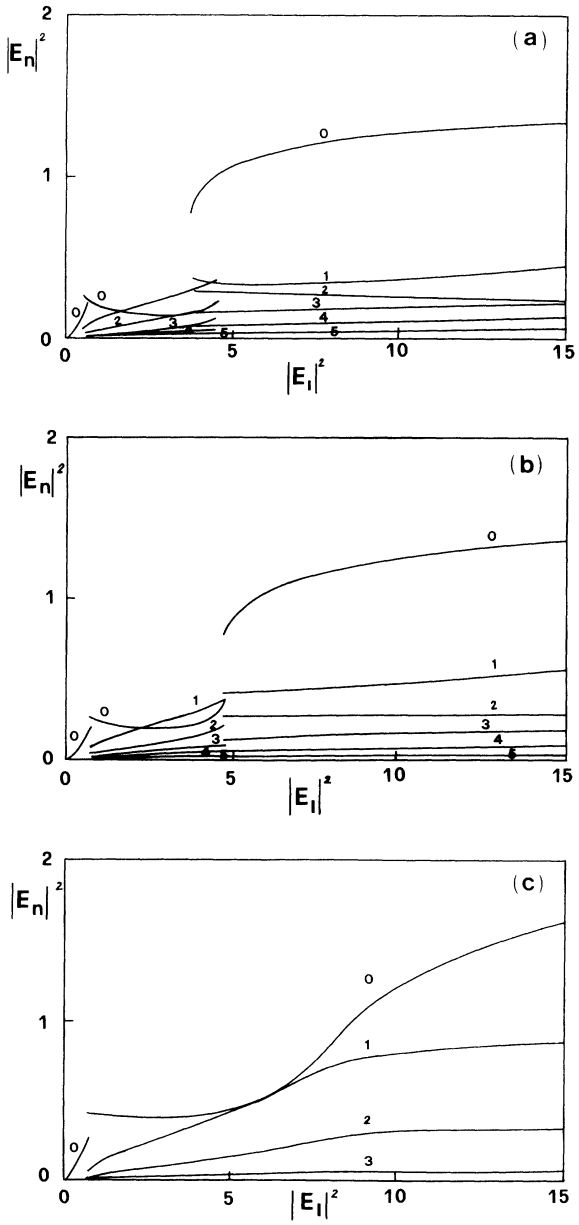

FIG. 11. Mode intensities as a function of input-field intensity of model 2, truncated to the first six modes. The parameters are $\bar{\eta}=-1$, $a=1.0$, and $\Theta=2.0$. The damping coefficients of the higher-order modes: (a) $\beta=0$, (b) $\beta=0.005$, and (c) $\beta=0.05$ [see Eq. (55)].

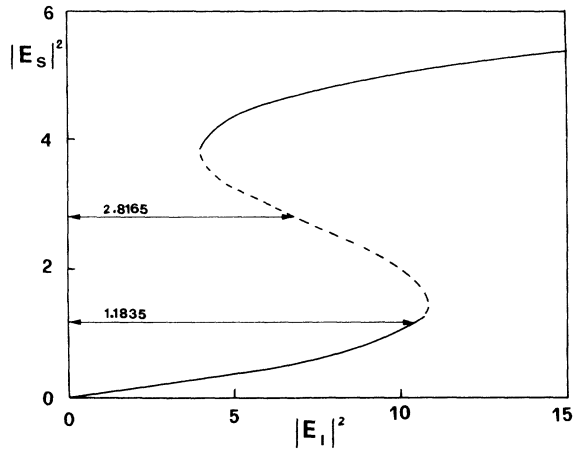

FIG. 12. The curve of steady-state solutions for self-defocusing case of model 1, truncated to the first three modes. The dashed line indicates the unstable region of these solutions. The arrows indicate the boundaries of the segment of the steady-state curve in which the mode $n=1$ is unstable. The parameters are $\bar{\eta}=-1$, $a\pi^2=1.0$, and $\Theta=4.0$. Between the two horizontal lines is an unstable region, susceptible to the growth of mode $n=1$, which overlaps with the unstable region of the negatively sloped portion of the steady-state curve of output intensity vs input intensity.

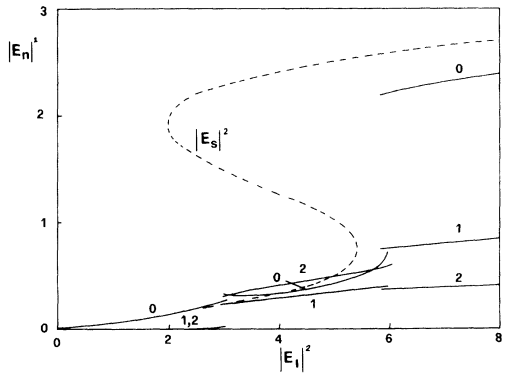

FIG. 13. Mode intensities as a function of input-field intensity for the self-defocusing case of model 2, truncated to the first three modes. The dashed line indicates the curve described by Eq. (54b). The parameters are $\bar{\eta}=-1$, $a=1.0$, and $\Theta=4.0$.

linear part of the atomic dispersion [see Eq. (18d)]. The third-order terms describe nonlinear dispersion and the coefficients reflect the spatial couplings and interactions between transverse modes.

For small input-field intensities the homogeneous stationary solution (or the approximately single-fundamental-mode solution for model 2) is stable. As the amplitude of the input field is increased, there are instabilities with the spontaneous formation of more complex stationary spatial patterns in both models. In this case, all the transverse modes do not arise with their frequencies of resonance in the linearized cavity, but rather they appear with the input frequency as their common operating frequency; this phenomenon is analogous to the cooperative frequency locking in a laser [14] and to the injection locking in a laser with injected signal. In the case of a Cartesian cavity configuration (model 1), the onset of an inhomogeneous state corresponds to the spontaneous breaking of the translational symmetry in space (Turing instability [42]) and of the parity symmetry.

In both models, there are basically two transition regions: one characterized by the emergence of modes different from the fundamental; the other characterized, in most cases, by the disappearance (or by a decrease, at least in an interval of input intensity) of the first mode in favor of higher-order modes and/or of the fundamental mode. For large enough detuning subcritical bifurcations occur in both models, and the hysteresis regions are enlarged with increasing detuning.

Between the two models, an apparent difference is the nature of their bifurcations. For model 1, the bifurcations are supercritical for small detuning, and then become subcritical as the detuning is increased. For model 2, soft bifurcations, which look like supercritical bifurcations, occur for small detunings, but are transformed into subcritical bifurcations for large enough detuning.

In conclusion, the increase of the detuning parameter leads to the appearance of bistability, as predicted by the single-mode theory, which includes only the fundamental mode. In our more complete theory, however, the hysteresis cycles which appear are essentially multimode, and their shape is completely different from that prescribed by the single-mode steady-state curve. Hysteresis phenomena of this kind have been recently observed in a sodium cell [43]; they cannot be adequately described, however, by our simple model, because atomic diffusion plays a relevant role in that case.

In our cubic model, phenomena of spontaneous oscillations appear only in the Cartesian case (Fig. 3). The qualitative differences are (i) that the frequencies of modes in the Cartesian model are unequally spaced while in the cylindrical model they are equally spaced; and (ii) that Γ_{nklm}'s for the Cartesian model are different from zero only for a few values of the indices, while for the cylindrical case Γ_{nklm}'s are widely distributed and dependent on all the indices. Hence the modes are more strongly coupled in the cylindrical case, while some modes can operate relatively independently of each other in the Cartesian model. This feature might be linked to the fact that in the cylindrical case the system approaches a state in which all the modes are locked to the input-field frequency. Another important element in this connection is that in this model the frequency spacing κa between adjacent transverse modes is on the order of the cavity linewidth κ; it is well known, in fact, that this condition is characteristic of cooperative frequency locking in lasers [14]. If the atomic dynamics had not been adiabatically eliminated, the onset of spontaneous oscillations in the output intensity would become easier when κa is on the order of the atomic linewidth $\gamma_\perp$ for $\kappa \ll \gamma_\perp$, because in this case the large intermode spacing would prevent the locking of the modes to the frequency of the input field (i.e., the modes $n>0$ would arise with their own frequencies through a kind of nonlinear parametric gain). However, in these approximate models we have not retained any difference in nonlinear dispersion that results from the different detunings of the modes from the center of the atomic line.

In all the numerical calculations illustrated in Sec. V, we selected $a\pi^2=1$ (Cartesian case) and $a=1$ (cylindrical case), but we expect that they do not depend on this choice in any substantial way. Our results show a strong asymmetry between the self-focusing case $\eta=1$ and the self-defocusing case $\eta=-1$. In the case of a cylindrical cavity with spherical mirrors, the symmetry can be restored by changing the sign of the parameter a; this corresponds to changing from a quasiplanar cavity ($a>0$) to a quasiconcentric cavity ($a<0$) [30]. In the case of the Cartesian cavity, instead, there is no apparent sense in taking $a<0$.

We observe finally that the behaviors predicted by our theory may undergo some change if the system is allowed to spontaneously break the cylindrical symmetry. The analysis of model 2 with inclusion of the cylindrically asymmetric modes will be the subject of future work.

ACKNOWLEDGMENTS

We are grateful to Lorenzo Narducci for several stimulating discussions. This research was carried out in the framework of the ESPRIT Basic Research Action 3260 "Transverse Optical Patterns" (TOPP).

APPENDIX A

The electric field $\mathbf{E}$ inside the cavity obeys the following boundary condition [see Fig. 1(b)]:

$$\mathbf{E}(\rho,-\tfrac{1}{2},t)=\sqrt{T}\,\mathbf{E}_{\rm in}+\mathcal{P}_{1\to 3}\mathbf{E}\left[\rho,\tfrac{1}{2},t-\frac{\mathcal{L}-L}{c}\right] \tag{A1}$$

where the operator $\mathcal{P}_{1\to 3}$ takes care of the reflections of the radiation beam by the two spherical mirrors of the cavity, and of the propagation from mirror 1 to mirror 3 [Fig. 1(b)]. By taking into account the relation

$$\frac{\boldsymbol{\mu}\cdot\mathbf{E}(\rho,\eta,t)}{\hbar}=\frac{(\gamma_\perp\gamma_\parallel)^{1/2}}{2}\{F(\rho,\eta,t)\exp[i(k_0L\eta-\omega_0t)]+\text{c.c.}\}\,, \tag{A2}$$

and Eq. (28) we obtain the boundary condition for the envelope F

$$F(\rho,-\tfrac{1}{2},t)=TYA_0(\rho,-\tfrac{1}{2})+\exp\left[i\omega_0\frac{\mathcal{L}}{c}\right]\mathcal{P}_{1\to 3'}F\left[\rho,\tfrac{1}{2},t-\frac{\mathcal{L}-L}{c}\right]. \tag{A3}$$

Hence if we introduce the expansion (23), Eq. (A3) becomes

$$\sum_n f_n\left[-\frac{1}{2},t\right]A_n\left[\rho,-\frac{1}{2}\right]=TYA_0\left[\rho,-\frac{1}{2}\right]+\exp\left[i\omega_0\frac{\mathcal{L}}{c}\right]\sum_n f_n\left[\frac{1}{2},t-\frac{\mathcal{L}-L}{c}\right]\mathcal{P}_{1\to 3'}A_n\left[\rho,\frac{1}{2}\right]. \tag{A4}$$

The modal functions A_n satisfy the field equation for an empty cavity without input field and with ideal mirrors (i.e., $R=1$). In this case the electric field obeys the boundary condition

$$\mathbf{E}(\rho,-\tfrac{1}{2},t)=\mathcal{P}_{1\to 3'}\mathbf{E}\left[\rho,\tfrac{1}{2},t\frac{\mathcal{L}-L}{c}\right], \tag{A5}$$

with

$$\mathcal{P}'_{1\to 3'}=R^{-1}\mathcal{P}_{1\to 3'}. \tag{A6}$$

If one sets

$$\frac{\boldsymbol{\mu}\cdot\mathbf{E}(\rho,\eta,t)}{\hbar}=\frac{(\gamma_\perp\gamma_\parallel)^{1/2}}{2}\{A_n(\rho,\eta)\exp[i(k_nL\eta-\omega_nt)]+\text{c.c.}\}, \tag{A7}$$

where ω_n is the frequency of mode n and $k_n=\omega_n/c$, the function $A_n(\rho,\eta)$ obeys Eq. (24). By inserting Eq. (A7) into Eq. (A5) and taking Eq. (A6) into account, we obtain

$$\mathcal{P}_{1\to 3'}A_n(\rho,\tfrac{1}{2})=R\exp\left[-i\omega_n\frac{\mathcal{L}}{c}\right]A_n(\rho,-\tfrac{1}{2}). \tag{A8}$$

Finally, by combining Eqs. (A4) and (A8), and taking the orthonormality relation (25) into account, we obtain at the boundary conditions for the modal amplitudes f_n

$$f_n\left[-\frac{1}{2},t\right]=TY\delta_{n,0}+\exp(-i\delta_n)Rf_n\left[\frac{1}{2},t-\frac{\mathcal{L}-L}{c}\right], \tag{A9}$$

where δ_n is defined by Eq. (29). Equation (A9) coincides with Eq. (27) if one takes into account that $\tau=\gamma_\perp t$.

APPENDIX B

Under the adiabatic and the cubic approximations, the atomic polarization inside the medium is

$$P'\approx\frac{(1-i\Delta)F'}{1+\Delta^2+|F'|^2}\approx\frac{-i}{\Delta}F'+\frac{i}{\Delta^3}F'|F'|^2, \tag{B1}$$

and outside the medium

$$P'=0. \tag{B2}$$

In the last step of Eq. (B1) we assume $|\Delta|\gg 1$. The integral in Eq. (40) becomes

$$I_n(\tau')\equiv I_n^{(1)}(\tau')+I_n^{(3)}(\tau'), \tag{B3}$$

where

$$I_n^{(1)}(\tau')\equiv\frac{-i}{\Delta}\frac{L}{L_A}\int_{-L_A/2L}^{L_A/2L}d\eta\exp[(\ln R-i\delta_n)(\eta+\tfrac{1}{2})]\int_0^\infty d\rho\,\rho A_n^*(\rho,\eta)F'(\rho,\eta,\tau') \tag{B4}$$

and

$$I_n^{(3)}(\tau')\equiv\frac{i}{\Delta^3}\frac{L}{L_A}\int_{-L_A/2L}^{L_A/2L}d\eta\exp[(\ln R-i\delta_n)(\eta+\tfrac{1}{2})]\int_0^\infty d\rho\,\rho A_n^*(\rho,\eta)F'(\rho,\eta,\tau')|F'(\rho,\eta,\tau')|^2. \tag{B5}$$

Using Eqs. (23), (32b), and (25), the linear part of the integral is

$$I_n^{(1)}(\tau')=\frac{-i}{\Delta}\frac{L}{L_A}\int_{-L_A/2L}^{L_A/2L}d\eta\exp[(\ln R-i\delta_n)(\eta+\tfrac{1}{2})]f'_n(\eta,\tau').$$

Using Eqs. (35), (44), and the uniform field limit $T\ll 1$, we obtain

$$I_n^{(1)}(\tau')=\frac{-iL}{\Delta L_A}\int_{-L_A/2L}^{L_A/2L}d\eta[\bar{f}_n(\eta,\tau')-TY\delta_{n,0}(\eta+\tfrac{1}{2})]=\frac{-iL}{\Delta L_A}\int_{-L_A/2L}^{L_A/2L}d\eta\,\bar{f}_n(\eta,\tau')=\frac{-i}{\Delta}f_n^{(0)}(\tau'). \tag{B6}$$

By following the same method, the nonlinear part of the integral is

$$I_n^{(3)}(\tau')=\frac{iL}{\Delta^3 L_A}\int_{-L_A/2L}^{L_A/2L}d\eta\exp[(\ln R-i\delta_n)(\eta+\tfrac{1}{2})]\int_0^\infty d\rho\,\rho A_n^*(\rho,\eta)$$
$$\times\sum_{klm}A_k(\rho,\eta)A_l(\rho,\eta)A_m^*(\rho,\eta)f_k'(\eta,\tau')f_1'(\eta,\tau')f_m'^*(\eta,\tau')$$
$$=\frac{iL}{\Delta^3 L_A}\int_{-L_A/2L}^{L_A/2L}d\eta\exp[-2(\eta+\tfrac{1}{2})\ln R-i(\eta+\tfrac{1}{2})(\delta_n-\delta_k-\delta_l+\delta_m)][\bar{f}_k(\eta,\tau')-TY\delta_{k,0}(\eta+\tfrac{1}{2})]$$
$$\times[\bar{f}_1(\eta,\tau')-TY\delta_{l,0}(\eta+\tfrac{1}{2})][\bar{f}_m^*(\eta,\tau')-TY\delta_{m,0}(\eta+\tfrac{1}{2})]$$
$$\times\int_0^\infty d\rho\,\rho A_n^*(\rho,\eta)A_k(\rho,\eta)A_l(\rho,\eta)A_m^*(\rho,\eta)\ .$$

By using the uniform field limit (14), Eq. (41), and Eq. (44), we have

$$I_n^{(3)}(\tau')\approx\frac{iL}{\Delta^3 L_A}\sum_{klm}f_k^{(0)}(\tau')f_l^{(0)}(\tau')f_m^{(0)*}(\tau')\int_{-L_A/2L}^{L_A/2L}d\eta\int_0^\infty d\rho\,\rho A_n^*(\rho,\eta)A_k(\rho,\eta)A_l(\rho,\eta)A_m^*(\rho,\eta)\ . \tag{B7}$$

For simplicity we assume the medium is thin enough so that the mode function $A_n(\rho,\eta)$ can be replaced by $A_n(\rho,0)$ (i.e., the length L_A is much smaller than the Rayleigh range); thus

$$I_n^{(3)}(\tau')\approx\frac{i}{\Delta^3}\sum_{klm}f_k^{(0)}(\tau')f_l^{(0)}(\tau')f_m^{(0)*}(\tau')\int_0^\infty d\rho\,\rho A_n^*(\rho,0)A_k(\rho,0)A_l(\rho,0)A_m^*(\rho,0)\ , \tag{B8}$$

where $A_n(\rho,0)$ is the real function

$$A_n(\rho,0)=\frac{2}{v_0}L_n\left[\frac{2\rho^2}{v_0^2}\right]\exp\left[-\frac{\rho^2}{v_0^2}\right]\ . \tag{B9}$$

Under the transformation $\bar{\rho}=\rho/v_0$, Eq. (B8) becomes

$$I_n^{(3)}(\tau')\approx\frac{i}{\Delta^3\eta_0}\sum_{klm}f_k^{(0)}(\tau')f_l^{(0)}(\tau')f_m^{(0)*}(\tau')\int_0^\infty d\bar{\rho}\,\bar{\rho}A_n^*(\bar{\rho})A_k(\bar{\rho})A_l(\bar{\rho})A_m^*(\bar{\rho})\ , \tag{B10}$$

where

$$\eta_0=v_0^2\ , \tag{B11}$$

$$A_n(\bar{\rho})=2L_n(2\bar{\rho}^2)\exp(-\bar{\rho}^2)\ . \tag{B12}$$

[1] Special issues of J. Opt. Soc. Am. B **2** (1) (1985); **5** (5) (1988); **7** (6) (1990); **7** (7) (1990).

[2] *Optical Instabilities,* edited by R. W. Boyd, M. G. Raymer, and L. M. Narducci (Cambridge University Press, Cambridge, 1986).

[3] *Optical Chaos,* edited by J. Chrostowski and N. B. Abraham, SPIE Proc. Vol. 667 (SPIE, Bellingham, WA, 1986).

[4] *Instabilities and Chaos in Quantum Optics,* edited by F. T. Arecchi and R. Harrison, Springer Series in Synergetics Vol. 34 (Springer-Verlag, Berlin, 1987).

[5] P. W. Milonni, J. R. Ackkerhalt, and M.-L. Shih, *Chaos in Laser-Matter Interactions* (World Scientific, Singapore, 1987).

[6] *Instabilities and Chaos in Quantum Optics II,* edited by N. B. Abraham, F. T. Arecchi, and L. A. Lugiato (Plenum, New York, 1988).

[7] N. B. Abraham, P. Mandel, and L. M. Narducci, in *Progress in Optics,* edited by E. Wolf (Elsevier, Amsterdam, 1988), Vol. XXV, p. 1.

[8] L. M. Narducci and N. B. Abraham, *Laser Physics and Laser Instabilities* (World Scientific, Singapore, 1988).

[9] *Dynamics of Nonlinear Optical Systems,* edited by F. J. Bermejo and L. Pesquera (World Scientific, Singapore, 1988).

[10] D. W. McLaughlin, J. V. Moloney, and A. C. Newell, Phys. Rev. Lett. **54**, 681 (1985).

[11] C. K. R. T. Jones and J. V. Moloney, Phys. Lett. A **117**, 175 (1986).

[12] L. A. Lugiato and R. Lefever, Phys. Rev. Lett. **58**, 220 (1987).

[13] M. Le Berre, E. Ressayre, A. Tallet, H. M. Gibbs, D. L. Kaplan, and M. H. Rose, Phys. Rev. A **35**, 4020 (1987).

[14] L. A. Lugiato, C. Oldano, and L. M. Narducci, J. Opt. Soc. Am. B **5**, 879 (1988).

[15] (a) L. A. Lugiato, L. M. Narducci, and R. Lefever, in *Lasers and Synergetics,* edited by R. Graham and A. Wunderlin, Springer Proceedings in Physics Vol. 19 (Springer-Verlag, Berlin, 1988), p. 53; (b) in *Synergetics, Order and Chaos,* edited by M. G. Velarde (World Scientifc, Singapore, 1988), p. 115.

[16] A. Ouarzeddini, H. Adachihara, J. V. Moloney, D. W. Mclaughlin, and A. C. Newell, J. Phys. (Paris) Colloq. **49**, C2-455 (1988).

[17] (a) L. A. Lugiato, C. Oldano, L. Sartirana, Wang Kaige, L. M. Narducci, G.-L. Oppo, F. Prati, and G. Broggi, in *Neural and Synergetic Computers,* edited by H. Haken,

Springer Series in Synergetics Vol. 42 (Springer-Verlag, Berlin, 1988), p. 242; (b) L. A. Lugiato, W. Kaige, L. M. Narducci, G.-L. Oppo, M. A. Pernigo, J. R. Tredicce, D. K. Bandy, and F. Prati, *ibid.*, p. 252.

[18] S. A. Akhmanov, M. A. Vorontsov, and V. Yu. Ivanov, Pis'ma Zh. Eksp. Teor. Fiz **47**, 611 (1988) [JETP Lett. **47**, 707 (1988)].

[19] G. Grynberg, E. Le Bihan, P. Verkerk, P. Simoneau, J. R. R. Leite, D. Bloch, S. Le Boiteux, and M. Ducloy, Opt. Commun. **67**, 363 (1988).

[20] J. R. Tredicce, E. J. Quel, A. M. Ghazzawi, C. Green, M. A. Pernigo, L. M. Narducci, and L. A. Lugiato, Phys. Rev. Lett. **62**, 1274 (1989).

[21] (a) R. Lefever, L. A. Lugiato, Wang Kaige, N. B. Abraham, and P. Mandel, in *Dynamics of Nonlinear Optical Systems* (Ref. [9]), p. 175; (b) Phys. Lett. A **135**, 254 (1989).

[22] (a) L. A. Lugiato and C. Oldano, Phys. Rev. A **37**, 3896 (1988); (b) M. Aguado and M. San Miguel, *ibid.* **37**, 450 (1988).

[23] L. A. Lugiato, F. Prati, L. M. Narducci, and G.-L. Oppo, Opt. Commun. **69**, 387 (1989).

[24] J. V. Moloney, H. Adachihara, R. Indik, C. Lizarraga, R. Northcutt, D. W. Mclaughlin, and A. C. Newell, J. Opt. Soc. Am. B **7**, 1039 (1990).

[25] Chr. Tamm and C. O. Weiss, Opt. Commun. **78**, 253 (1990).

[26] H. Lin and N. B. Abraham, Opt. Commun. **79**, 476 (1990).

[27] W. J. Firth, J. Mod. Opt. **37**, 151 (1990).

[28] W. J. Firth and C. Paré, Opt. Lett. **13**, 1096 (1988).

[29] W. J. Firth, C. Penman, and C. Paré, Opt. Commun. **75**, 136 (1990).

[30] L. A. Lugiato, G. L. Oppo, J. R. Tredicce, L. M. Narducci, and M. A. Pernigo, J. Opt. Soc. Am. B **7**, 1019 (1990).

[31] P. Coullet, L. Gil, and F. Rocca, Opt. Commun. **73**, 403 (1989).

[32] F. T. Arecchi, R. Meucci, and L. Pezzati, Phys. Rev. A **42**, 2531 (1990).

[33] F. T. Arecchi, G. Giacomelli, P. L. Ramazza, and S. Residori, Phys. Rev. Lett. **65**, 2531 (1990).

[34] C. Green, G. B. Mindlin, E. J. D'Angelo, H. G. Solari, and J. R. Tredicce, Phys. Rev. Lett. **65**, 3124 (1990).

[35] M. Brambilla, F. Battipede, L. A. Lugiato, V. Penna, F. Prati, C. Tamm, and C. O. Weiss, Phys. Rev. A **43**, 5090 (1991); **43**, 5114 (1991).

[36] L. A. Lugiato, F. Prati, L. M. Narducci, P. Ru, J. R. Tredicce, and D. K. Bandy, Phys. Rev. A **37**, 3847 (1988).

[37] (a) P. Ru, L. M. Narducci, J. R. Tredicce, D. K. Bandy, and L. A. Lugiato, Opt. Commun. **63**, 310 (1987); (b) A. Yariv, *Optical Waves in Crystals* (Wiley, New York, 1984).

[38] M. Brambilla, F. Castelli, L. A. Lugiato, F. Prati, and G. Strini, Opt. Commun. **83**, 367 (1991).

[39] Of course, condition (41) cannot hold for all values of n. We assume that it is valid for the values of n that are relevant for the dynamics of the system.

[40] H. M. Gibbs, S. L. McCall, and T. N. C. Venkatesan, Phys. Rev. Lett. **36**, 1135 (1976).

[41] M. Aguado, R. F. Rodriguez, and M. San Miguel, Phys. Rev. A **39**, 5686 (1989).

[42] A. M. Turing, Philos. Trans. R. Soc. London Ser. B **237**, 37 (1952).

[43] J. Nalik, L. Hoffer, G. L. Lippi, Ch. Vorgerd, and W. Lange, Phys. Rev. A **45**, R4237 (1992).

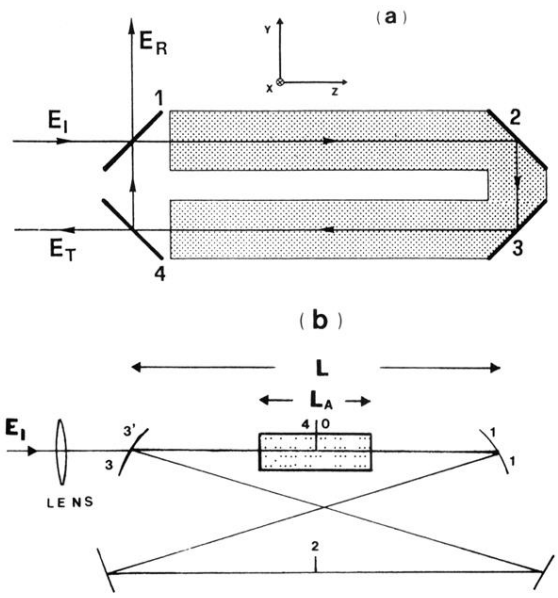

FIG. 1. Schematic representations of the ring cavities. (a) Model 1: Cartesian geometry; (b) model 2: cylindrical geometry, where 1′ and 3′ indicate the positions after reflection from the mirrors.